Proceedings of the 28th IEEE
EMBS Annual International Conference
New York City, USA, Aug 30-Sept 3, 2006

Quantitative wavelet domain image processing of dynamic PET data

Kjell Erlandsson, *Member, IEEE*, Yinpeng Jin, Andrew T. Wong, Peter D. Esser, Andrew F. Laine, R. Todd Ogden, Maria A. Oquendo, Ronald van Heertum, J. John Mann, Ramin V. Parsey

Abstract— **Neuroreceptor PET studies consisting of long dynamic data acquisitions result in data with low signal-to-noise ratio and limited spatial resolution. To address these problems we have developed a 3D wavelet-based image processing tool (wavelet filter, WF), containing both denoising and enhancement functionality. The filter is based on multi-scale thresholding and cross-scale regularization. These operations are data-driven, which may lead to non-linearity effects and hamper quantification of dynamic PET data. The aim of the present study was to investigate these effects using both phantom and human PET data. A phantom study was performed with a cylindrical phantom, filled with ^{18}F, containing a number of spherical inserts filled with ^{11}C. Human studies were performed on 9 healthy volunteers after injection of the serotonine transporter tracer [^{11}C]DASB. Images from both phantom and human studies were reconstructed with filtered backprojection and post-processed by WF with a series of different denoising and enhancement parameter values. The phantom study was analyzed by computing the insert-to-background ratio as a function of time. The human study was analyzed with a 1-tissue compartment model for a series of brain regions. For the phantom study, linear relations were found between unprocessed and WF processed data for positive contrasts. However, for negative contrast, non-linearity effects were observed. For the human data, good correlation was obtained between results from unprocessed and WF processed data. Our results showed that, although non-linear effects may appear in low-contrast areas, it is possible to achieve accurate quantification with wavelet-based image processing.**

I. Introduction

Dynamic PET and SPECT data generally suffer from low signal-to-noise and limited spatial resolution. Kinetic modeling methods used for analyzing these data are often sensitive to noise and therefore some kind of noise reduction technique is required. This can be done either by averaging the image data over predefined volumes of interest (VOIs) before performing the kinetic analysis, or by applying a denoising filter to the data. Traditional denoising filters are associated with degradation of spatial resolution. Wavelet-based filters, on the other hand, have the potential to reduce noise while preserving spatial resolution due to its ability to provide both space and frequency localization.

A wavelet-based 3D image processing tool for PET and SPECT images has been developed by our group [1]-[4], which can be used for noise-reduction (denoising) as well as for sharpening of image details (enhancement). The wavelet-filter (WF) is based on multi-scale thresholding and cross-scale regularization, and utilizes information from the image itself. This data-dependency may lead to non-linearity effects that could hamper quantification of dynamic PET or SPECT data. The aim of the present study was to investigate the practical implications of these using dynamic PET data from both phantom and human studies.

Wavelet-based processing of dynamic PET data has been used by other groups in either the spatial domain [5]-[8], the temporal domain [9]-[10] or both [11], leading to improvements in the final results. However, since the characteristics of filter algorithms may depend on the implementation details in each case, general conclusions regarding the applicability of wavelet-based filters cannot be drawn from these studies. We have evaluated the characteristics of one particular WF [1]-[4] using VOI-based analysis of dynamic PET data with the ultimate goal of achieving improved results from voxel-based analysis.

II. Materials and Methods

A. Wavelet filter

The WF algorithm is based on a dyadic wavelet transform [12], using the first derivative of a cubic spline function as the wavelet basis. Conventional multi-scale thresholding was generalized so that each sub-band is processed with a distinct thesholding operator. Effective de-noising and signal recovering was achieved using a cross-scale regularization process, in which detailed signal features within multi-scale sub-bands are recovered by estimating edge locations from coarser levels within the wavelet expansion. The thesholding operator was applied to the modulus of wavelet coefficients, rather than to individual components, which provides more accurate orientation selectivity.

Manuscript received April 24, 2006. This work was supported in part by Siemens Medical Solutions (USA).

K. Erlandsson is with the Departments of Psychiatry and Radiology, Columbia University, New York, NY. (Address for correspondence: NYSPI, 1051 Riverside Drive, Box 42, New York, NY 10032, USA; email: kjell@neuron.cpmc.columbia.edu)

Y. Jin was with the Department of Biomedical Engineering, Columbia University, New York, NY, now with Constellation Energy Commodities Group, MD.

A. T. Wong is with the Department of Psychiatry Columbia University, New York, NY.

P. D. Esser and R. van Heertum are with the Department of Radiology, Columbia University, New York, NY.

A. Laine is with the Departments of Biomedical Engineering and Radiology, Columbia University, New York, NY.

R. T. Ogden is with the Department of Psychiatry, Columbia University, New York, NY, the Department of Biostatistics, Mailman School of Public Health, Columbia University, New York, NY, and the Department of Neuroscience, New York State Psychiatric Institute, New York, NY.

M. A. Oquendo, J. J. Mann and R. V. Parsey are with the Department of Psychiatry, Columbia University, New York, NY and with the Department of Neuroscience, New York State Psychiatric Institute, New York, NY.

B. Phantom study

A phantom study was performed on an ECAT HR+ PET scanner (Siemens, Knoxville, TN). A cylindrical phantom containing a number of spherical inserts (diameters 10, 12, 16, 20, 25, 31 mm) was used. The background was filled with ^{18}F ($T_{1/2}$=110 min) and the inserts with ^{11}C ($T_{1/2}$=20 min). Dynamic PET data were acquired in 5-min time-frames over a period of 4 hours. Due to the difference in half-lives of the 2 radionuclides, the insert-to-background activity concentration ratio decreased over the time of the experiment. The PET data was corrected for scatter and attenuation and images were reconstructed by filtered backprojection (FBP) using the Shepp filter with cut-off at the Nyquist frequency. The images were then processed by WF using various combinations of 2 parameters determining the amount of denoising (D) and enhancement (E), respectively: D/E={1/1, 2/2, 3/3, 5/5}. The mean image value in each sphere was studied as a function of time.

C. Human PET studies

Six healthy volunteers were injected with the serotonin transporter tracer [^{11}C]DASB, and dynamic PET data were acquired on an ECAT HR+ scanner (Siemens, Knoxville, TN) over a period of 2 hours from the time of injection. Data were acquired in time-frames of 3x20 s, 3x1 min, 3x2 min, 2x5 min, and 10x10 min. Arterial blood samples were taken and the concentration of parent tracer in plasma was determined [13] for use as an input function in kinetic modeling. These subjects were part of a larger study approved by the Institutional Review Boards of Columbia University Medical Center and the New York State Psychiatric Institute [13].

The PET data was corrected for scatter and attenuation and images were reconstructed by FBP using the Shepp filter with cut-off at the Nyquist frequency. The reconstructed images were corrected for motion by realignment, and co-registered to a structural MRI image, obtained for each subject. Volumes of interest (VOIs) were drawn on the MRI images and then applied to the PET images to generate time-activity curves (TACs). VOIs were drawn for the following regions: anterior cingulate, amygdala, cerebellar cortex, cingulate, dorsal caudate, dorso-lateral prefrontal cortex, dorsal putamen, entorinal cortex, hippocampus, inferior anterior cingulate, insula, medial prefrontal cortex, midbrain, occipital cortex, orbital cortex, parietal cortex, parahippocampus, posterior parahippocampus, superior anterior cingulate, temporal cortex, thalamus, uncus and ventral striatum.

Tracer binding in each VOI was quantified by kinetic analysis of the TACs using a 1-tissue compartment model based on the measured arterial input function. In a previous study, comparing different methods for modeling [^{11}C]DASB data, this method was shown to be the best one for voxel-based analysis [14]. The total volume of distribution was calculated as: $V_T=K_1/k_2$, where K_1 and k_2 are first order rate constants describing transfer of tracer from plasma to tissue and from tissue to plasma, respectively. Binding potential was defined as: $BP_2=(V_T-V_R)/V_R$, where V_R is the V_T value in the reference region (cerebellar gray matter). The weighted sum of squared residuals (WRSS) was calculated for each fitted TAC.

Kinetic analysis was performed before and after WF processing of the reconstructed images with different combinations of denoising and enhancement parameters: D/E={1.5/0, 1.5/15, 3/0, 3/15}. The V_T and BP_2 values obtained after WF processing were compared with the ones obtained from the unprocessed data by linear correlation analysis.

III. Results

A. Phantom data

Selected images of unprocessed and WF processed sections through the center of the spheres of the phantom study are shown in Fig. 1. Data from 3 different time-points are shown, corresponding to high and low positive contrast as well as negative contrast. With positive contrast, a significant amount of smoothing of the background is achieved with WF, while the spheres appear unaffected. With negative contrast, the cold spheres are visually more distinct after WF processing.

Fig. 2 shows results from the quantitative analysis of the phantom study. The mean value in each sphere as well as in the background was plotted as a function of time in semi-logarithmic graphs. Due to the exponential decay of ^{11}C, straight lines should be obtained in theory. The data was corrected for the decay of ^{18}F, so the background is at a constant level. For unprocessed data the lines are straight and parallel when the contrast is positive. With negative contrast, the curves get closer together as a result of contribution from the background (partial volume effects), which is more significant for smaller spheres. For the WF processed data the lines are also straight and parallel with positive contrast. However, at negative contrast, the curves clearly bend and become more horizontal. This is an indication of non-linearity.

B. Human data

Selected images from one of the human [^{11}C]DASB PET studies are shown in Fig. 3. Coronal images from one short (1 min) and one long (10 min) time frame are shown, unprocessed and after WF processing with denoising only (D/E=3/0) and with both denoising and enhancement (D/E=3/15). With denoising only, the 1-min frame becomes visibly much smoother, while the 10-min frame remains almost unaffected. This illustrates the data-dependency of the filter; the amount of smoothing applied is a function of the amount of noise present in the image. When enhancement is included in the WF processing, this leads to noise-amplification in the 1-min frame, while the 10-min image becomes much sharper and with increased contrast as a result of the enhancement of the true signal.

Tables I and II show the results of the correlation analysis between WF processed and unprocessed data for V_T and BP_2, respectively, obtained using all VOIs in all subjects. Fig. 4 shows the WF processed V_T values as a function of the unprocessed ones, for WF denoising only (D/E=3/0) and both denoising and enhancement (D/E=3/15). There is good correlation (large R^2 values) and in all cases. For the V_T values, there is a good agreement (small intercept and slope close to 1) when denoising only is used. With enhancement included, the slope is >1, which is an expected effect of improved resolution and a reduction of partial volume effects. For the BP_2 values, which are based on the ratio between V_T values for 2 different regions, the slope is close to 1 both with and without enhancement.

Table 3 shows the WRSS for each set of WF parameter, averaged across VOIs and subjects and normalized to the unprocessed values. With denoising only, WRSS is reduced, although only marginally for the lower denoising parameter value (D=0.15). With both denoising and enhancement, WRSS increases due to noise-amplification.

IV. Discussion and Conclusions

We have developed a wavelet domain image processing algorithm based on multi-scale thresholding and cross-scale regularization. The filter was designed in order to address two main limitations in dynamic PET studies: low SNR and limited spatial resolution. We have evaluated this algorithm using dynamic phantom as well as human PET data. The results from the phantom study showed that, while linearity was preserved with high contrast, WF processing could lead to non-linear effects in areas with low contrast. The results from the human studies showed that WF processing of real data could lead to quantitatively accurate values while reducing noise and/or enhancing image details.

Having confirmed the linearity of the WF algorithm on a VOI basis, our next step will be to investigate if this method would be beneficial for voxel-based image analysis.

Acknowledgments

We would like to thank the employees of the Brain Imaging Core of the NIMH-funded Conte Translational Neuroscience Center, the Kreitchman PET Center, and the Columbia University Radioligand Laboratory for expert help.

References

[1] Y. Jin, P. D. Esser, R. L. Van Heertum, A. F. Laine, "Evaluation of Multi-scale Regularized Tomographic Reconstruction of PET Brain Scans", *J Nucl Med* **46**(5):165P, 2005.

[2] Y. Jin, P. D. Esser, T. Aikawa, B. Kuang, S. Duan, A. F. Laine, "Regularization of PET Reconstruction Using Multi-scale Adaptive Thresholding", 26th Annual International Conference IEEE Engineering in Medicine and Biology Society (EMBS), September 1-5, 2004 SanFrancisco, California.

[3] Y. Jin, E.D. Angelini, P.D. Esser, A.F. Laine, "De-noising SPECT/PET images using cross-scale regularization", MICCAI'03, Montreal, Canada, Nov. 2003. pp. Part II 32-40.

[4] J. Kalifa, A.F. Laine, P.D. Esser, "Regularization in tomographic reconstruction using thresholding estimators," IEEE Trans. Med. Im., Vol. 22, pp. 351 -359, 2003.

[5] F. E. Turkheimer, M. Brett, D. Visvikis, and V. J. Cunningham, "Multiresolution analysis of emission tomography images in the wavelet domain," *J Cereb Blood Flow Metab*, vol. 19, pp. 1189-208, 1999.

[6] F. E. Turkheimer, R. B. Banati, D. Visvikis, J. A. Aston, R. N. Gunn, and V. J. Cunningham, "Modeling dynamic PET-SPECT studies in the wavelet domain," *J Cereb Blood Flow Metab*, vol. 20, pp. 879-93, 2000.

[7] F. E. Turkheimer, J. A. Aston, R. B. Banati, C. Riddell, and V. J. Cunningham, "A linear wavelet filter for parametric imaging with dynamic PET," *IEEE Trans Med Imaging*, vol. 22, pp. 289-301, 2003.

[8] Z. Cselenyi, H. Olsson, L. Farde, and B. Gulyas, "Wavelet-aided parametric mapping of cerebral dopamine D2 receptors using the high affinity PET radioligand [11C]FLB 457," *Neuroimage*, vol. 17, pp. 47-60, 2002.

[9] P. Millet, V. Ibanez, J. Delforge, S. Pappata, and J. Guimon, "Wavelet analysis of dynamic PET data: application to the parametric imaging of benzodiazepine receptor concentration," *Neuroimage*, vol. 11, pp. 458-72, 2000.

[10] M. Yaqub, R. Boellaard, M. Kropholler, M. Lubberink, and A. Lammertsma, "Improving accuracy and precision of PET pharmacokinetic analysis using wavelet based denoising of time activity curves," *J Cereb Blood Flow Metab*, vol. 25, pp. S640, 2005.

[11] N. M. Alpert, A. Reilhac, T. C. Chio, and I. Selesnick, "Optimization of dynamic measurement of receptor kinetics by wavelet denoising," *Neuroimage*, vol. 30, pp. 444-51, 2006.

[12] S. Mallat, S. Zhong, "Characterization of signals from multi-scale edges", IEEE Trans. Pattern Analysis and Machine Intelligence, Vol. 14, pp. 710-32, 1992.

[13] R. V. Parsey, J. M. Kent, M. A. Oquendo, M. C. Richards, M. Pratap, T. B. Cooper, V. Arango, and J. J. Mann, "Acute Occupancy of Brain Serotonin Transporter by Sertraline as Measured by [(11)C]DASB and Positron Emission Tomography," Biol Psychiatry, vol. 59, pp. 821-8, 2006.

[14] R. T. Ogden, A. Ojha, K. Erlandsson, M. A. Oquendo, J. J. Mann, and R. V. Parsey, "In vivo quantification of serotonin transporters using [(11)C]DASB and positron emission tomography in humans: modeling considerations," J Cereb Blood Flow Metab, 2006.

TABLE I.
CORRELATION BETWEEN V_T VALUES FROM UNPROCESSED AND WF PROCESSED DATA

De-noising	Enhancement	Slope	Intercept	R^2
0.15	0	1.003	0.043	1.000
0.3	0	0.994	0.093	1.000
0.15	15	1.062	0.238	0.996
0.3	15	1.056	0.301	0.997

TABLE II.
CORRELATION BETWEEN BP_2 VALUES FROM UNPROCESSED AND WF PROCESSED DATA

De-noising	Enhancement	Slope	Intercept	R^2
0.15	0	1.003	0.001	1.000
0.3	0	1.003	0.004	0.999
0.15	15	1.014	0.015	0.996
0.3	15	1.014	0.018	0.996

TABLE III.
WEIGHTED RESIDUAL SUM OF SQUARES AVERAGED ACROSS VOIS AND SUBJECTS

De-noising	Enhancement	WRSS*
0.15	0	0.987
0.3	0	0.880
0.15	15	1.284
0.3	15	1.172

*Normalized to unprocessed data

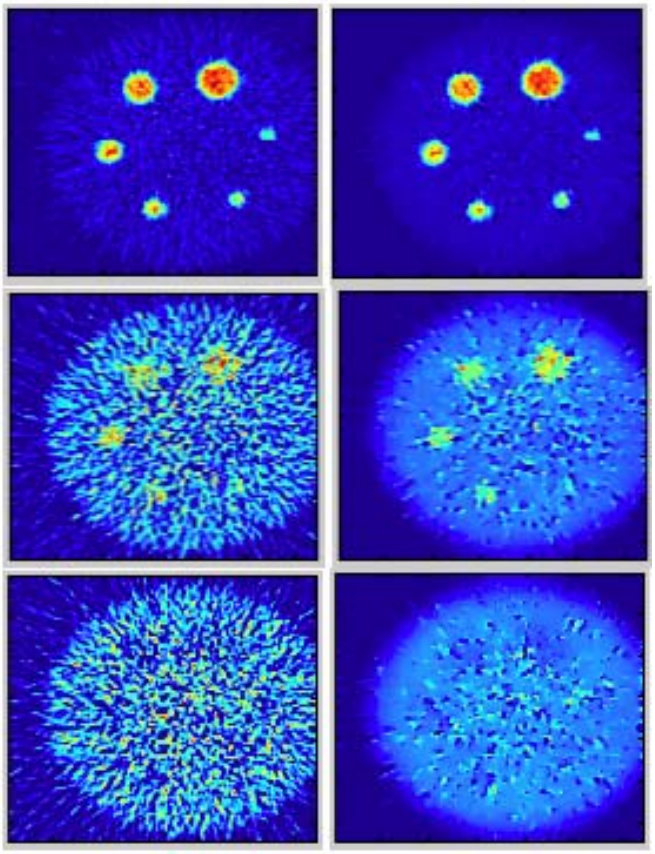

Fig. 1. The different time frames from a phantom study; unprocessed (left column) and WF processed (right column).

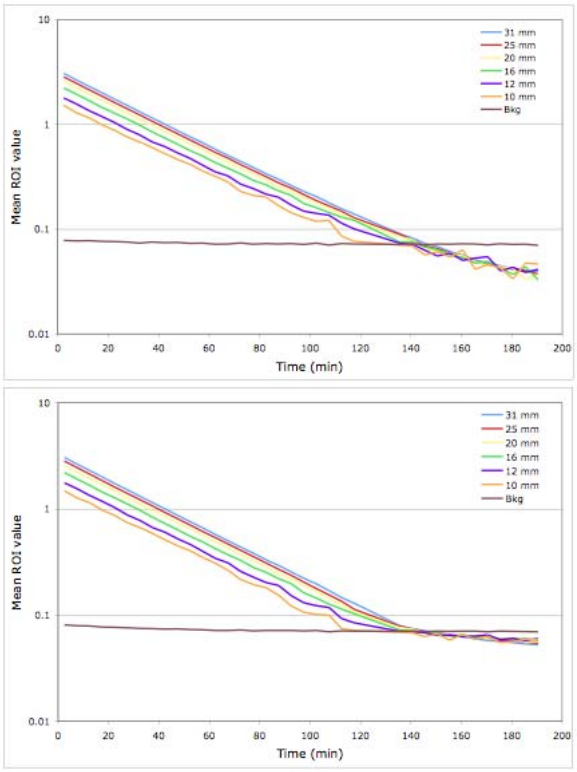

Fig. 2. Mean value in spherical inserts and background in the phantom study as a function of time; unprocessed data (top), WF processed data (bottom).

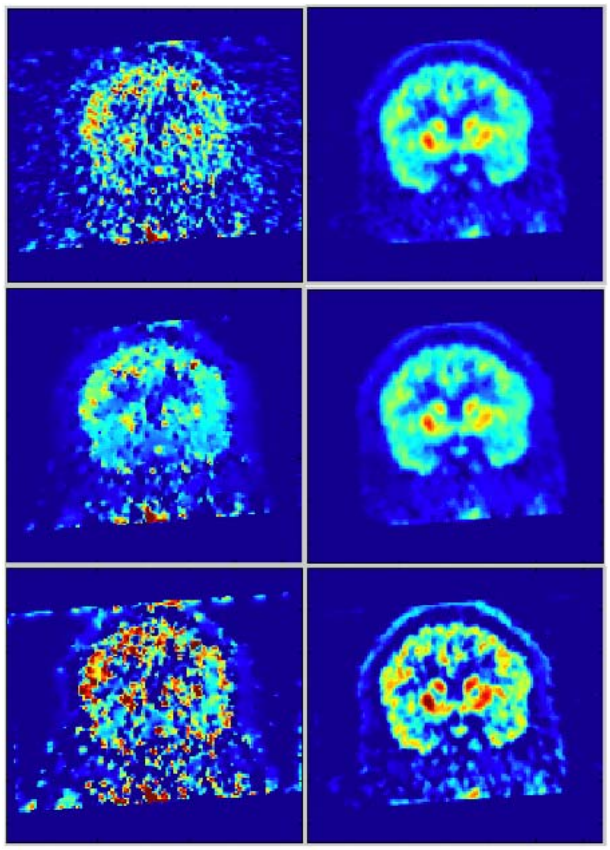

Fig. 3. Coronal sections from a human study, including a 1-min frame (left) and a 10-min time frame (right); unprocessed data (top row), WF denoising only (middle row), and WF denoising/enhancement (bottom row).

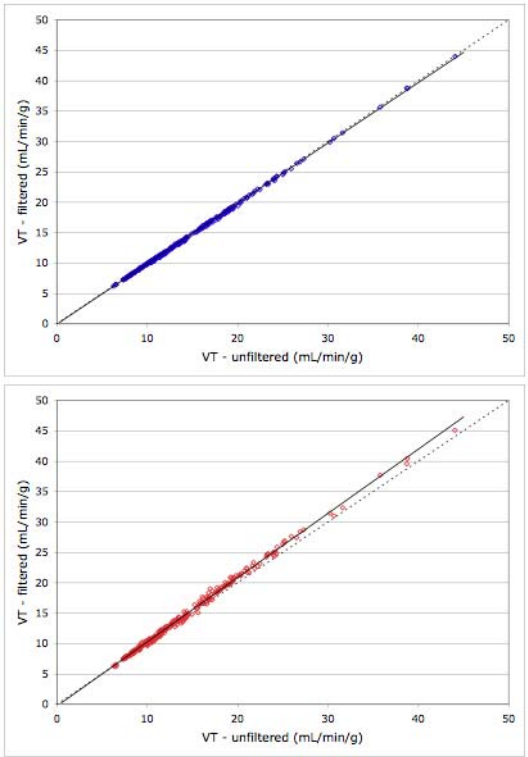

Fig. 4. Correlation between VT values obtained from unprocessed and WF processed data in the human studies; D/E=3/0 (top), D/E=3/15 (bottom). The dotted lines indicate the line of identity.